We are IntechOpen,
the world's leading publisher of
Open Access books
Built by scientists, for scientists

6,900
Open access books available

186,000
International authors and editors

200M
Downloads

Our authors are among the

154
Countries delivered to

TOP 1%
most cited scientists

12.2%
Contributors from top 500 universities

CLARIVATE ANALYTICS
BOOK CITATION INDEX
INDEXED

WEB OF SCIENCE™

Selection of our books indexed in the Book Citation Index
in Web of Science™ Core Collection (BKCI)

Interested in publishing with us?
Contact book.department@intechopen.com

Numbers displayed above are based on latest data collected.
For more information visit www.intechopen.com

Magnetic Nanoparticles as MRI Contrast Agents

Bashar Issa and Ihab M. Obaidat

Abstract

Magnetic Resonance Imaging (MRI) is a non-invasive imaging modality that offers both anatomical and functional information. Intrinsic longitudinal and transverse relaxation times (T_1 and T_2, respectively) provide tools to manipulate image contrast. Additional control is yielded when paramagnetic and magnetic particulate materials are used as contrast materials. Superparamagnetic particles are mostly synthesized from iron oxide and are usually coated with polymers and functional particles to offer multifunctional biomedical applications. The latter include not only MRI but also cancer treatment through drug delivery and hyperthermia. This Chapter reviews the fundamental dipole–dipole diamagnetic proton relaxation mechanism dominant in water followed by a brief description of the use of gadolinium complexes as MRI contrast agent. Finally, a description of the important chemical and physical properties of magnetic nanoparticle (MNP) that define their use as MRI relaxation enhancing agents especially for T_2. The main governing models are described for the different motional regimes with few simulation results demonstrating the applicability of the given equations.

Keywords: MRI, contrast agent, nanoparticle, magnetic moment, relaxation, T_1, T_2, dipole–dipole, superparamagnetism

1. Introduction

Relaxation in Nuclear Magnetic Resonance (NMR) Spectroscopy or more relevant to this Chapter Magnetic Resonance Imaging (MRI) plays a pivotal role in the selection of experimental parameters and indeed in the image contrast. The emphasis in MRI is on longitudinal (spin–lattice) and transverse (spin–spin) relaxation times (T_1 and T_2, respectively). The advent in technology and the spread of higher field strength magnets made available a wealth of imaging pulse sequences that rely on the manipulation of T_1 and T_2 weighting to produce different diagnostic information. Early quantification of relaxation times in biological tissues hoped to find consistent differences in their values between malignant tumors and normal tissues [1]. This was based on the different abilities of water to move and sample different structural environments present due to the development of cancer. It was argued then that water content is larger in cancerous cells and water molecules are more loosely connected, however, alternative interpretations soon emerged. Nowadays various human tissues exhibit different relaxation times and it is these differences that are utilized in the wealth of experimental imaging sequences to produce different image contrast and details.

A brief introduction of MRI relaxation is given below which includes the phenomenological description, the mechanism responsible for relaxation as modulated by molecular motions before describing in more details relaxation enhancement by paramagnetic complexes. This leads the way to our main topic which is the enhancement of relaxation caused by the presence of magnetic nanoparticles (MNP).

2. Phenomenological equations of relaxation

NMR relaxation is the process by which magnetic spins return to their thermal equilibrium (Boltzmann distribution) state prior to a disturbance which is usually caused by the absorption of energy in the form of a radio frequency (RF) pulse or when the spin system is placed in a uniform magnetic field [2]. The spins return to their preferential alignment along the direction of the static magnetic field (B_0) by exchanging energy with the surrounding thermal reservoir, also known as the lattice. The latter can include spins that are physically located in the same molecule (e.g. the two hydrogen atoms in a water molecule), neighboring molecules, or solvent molecules. This process is known as spin–lattice, longitudinal or T_1 relaxation which reestablishes the state of spin polarization characterized by a net magnetization (M_0). The net magnetization depends on the strength of the magnetic field (B_0), nuclear spin (I), the gyromagnetic ratio (γ), and inversely on temperature. For a spin half (I = ½) system T_1 relaxation reduces the energy of the system because spins undergo a quantum transition from the high energy level to the lower one with energy difference given by the fundamental equation

$$\Delta E = h\omega_0/2\pi = \frac{\gamma h B_0}{2\pi} \tag{1}$$

Or

$$\omega_0 = \gamma B_0 \tag{2}$$

The Larmor frequency (ω_0) is the frequency of the quantized released electromagnetic energy, and h is Planck's constant. Both T_1 relaxation and the RF excitation involve the same frequency given above. The phenomenological equation describing the growth of the longitudinal magnetization M_z from the initial value $M_z(0)$ is a first order process given by (in the rotating frame)

$$\frac{dM_z}{dt} = -\frac{(M_0 - M_z)}{T_1} \tag{3}$$

with solution

$$M_z(t) = M_z(0) \exp\left(-t/T_1\right) + M_0(1 - \exp\left(-t/T_1\right)) \tag{4}$$

For liquids at room temperatures the protons relaxation times are in the range 0.1–10 s.

If the RF excitation pulse produces 90° nutation of the longitudinal magnetization, then phase coherence is established between the spins and all of them point in one direction yielding transverse magnetization M_{xy}. The lifetime of this non-zero magnetization component is characterized by a time constant referred to as spin–spin or T_2 relaxation time. Immediately after the end of the RF pulse the spins start interacting with their neighbors by exchanging energy in non-dissipative manner,

unlike T_1, without net transfer to the lattice (in fact relaxation occurs during the RF pulse as well but we assume that the RF pulse duration is much shorter than T_2 relaxation). The coherence established by the RF pulse starts diminishing and the spins develop phase difference between them in the xy-plane. T_2 relaxation is related to T_1 relaxation since an increase in the longitudinal magnetization is not possible without a decrease in the transverse component, therefore, $T_2 \leq T_1$. For small molecules and large water pools that can approach bulk water T_2 values are in the range 10 ms–10 s. For solids it can be much shorter.

The phenomenological description for the transverse relaxation can also be described by a first order equation (in the rotating frame)

$$\frac{dM_{xy}}{dt} = -\frac{M_{xy}}{T_2} \tag{5}$$

leading to a solution

$$M_{xy}(t) = M_{xy}(0) \exp(-t/T_2) \tag{6}$$

This single exponential solution applies well for weak or non-interacting spins. For protons decaying in biological environments containing restrictions and molecules of various sizes the decay is non-exponential but often better described by a two exponential model reflecting compartments and exchange processes. The decay in ice is better described by a Gaussian rather than exponential process [2].

3. Relaxation mechanisms and molecular motion

Transitions between energy states, whether excitation or relaxation, are caused by oscillating magnetic fields. For resonance absorption conditions, the perturbing magnetic fields have to be oscillating at the Larmor frequency (ω_0). Other mechanisms at producing magnetic fields not only at ω_0 but also at zero and double the frequency ($2\omega_0$) will also be effective. This can be explained using arguments similar to Doppler effect [3] or more rigorously using quantum mechanics selection rules [2]. These fluctuations are produced mainly by molecular motion of the neighboring spins and by electronic excitations of paramagnetic atoms. Molecular motion modulated field fluctuations ($\vec{B}_{fluctuating}$) are dependent on the size of the nuclear spin, the environment and the presence of macromolecules, and temperature. One of the most important mechanisms is dipole–dipole interaction with a strength proportional to (μ/r^3) where μ is the magnetic moment and r is the distance between the two spins. This interaction contributes significantly to T_1 and T_2 relaxation through a distribution of molecular motional frequencies which is introduced next.

Molecules change their state of motion (typically within an average correlation time $\tau_C \sim 10^{-14}$–10^{-12} s for non-viscous fluids) due to interactions or collisions with neighboring molecules. For example, $\tau_C = 3.5 \times 10^{-12}$ s for liquid water at 20° C, while it increases significantly beyond this range for solids such as ice where $\tau_C = 2.0 \times 10^{-6}$ s. The frequencies describing water's state of motion will span the range 0–10^{12} Hz and, therefore, microscopic magnetic fields will be fluctuating at all these frequencies. The effect of these magnetic fields will be analogous to that of the RF pulse used in the excitation through the associated torque. Simple analysis of the cross-product equation for the torque experienced by the magnetization in the rotating frame $(\vec{B}_{fluctuating} \times \vec{M})_{rot}$ shows clearly that fluctuating magnetic field

components along the x- and y-directions (i.e. high frequency components since static components in the rotating frame are actually time varying in the laboratory frame) affect both T_1 and T_2 relaxation. Components along the z-direction, however, contribute to changing transverse magnetization, i.e. T_2 processes only [4]. This is so since longitudinal field component that is static in the rotating frame is also static in the laboratory frame. These are process involve zero frequency change i.e. no net energy transfer.

When looking at the average or ensemble of molecular motion where molecules can be moving with a range of frequencies, we also need to consider the strength or equivalently the Fourier component of the motion at each particular frequency. The correlation time (τ_C) plays the role of phase memory time for which a molecule "remembers" its state of motion in a similar fashion to the role of T_2 relaxation time. The Fourier transform of the Free Induction Decay (FID) NMR signal or the decay of the transverse magnetization yields the NMR Spectrum i.e. the strength of the magnetization at a particular frequency. This leads, in a more quantitative manner, to a simple assumption about the autocorrelation function $K(\tau)$ of each magnetic field component as being a single exponential function with a time constant τ_C. [5, 6] This can be derived by considering averaging over time the product of magnetic variations ($< \Delta B_i(t) \, \Delta B_j(t) >$) experienced by hydrogen two atoms as they experience tumbling rotations in the same water molecule. This motion produces variations in the angle joining the two atoms with respect to the applied field while the inter-atomic distance does not change. Assuming that the molecules are almost spherical that undergo isotropic tumbling simplifies the analysis considerably.

For a system of short τ_C then the fast decaying $K(\tau)$ tells that molecules lose their memory of relative position to neighboring molecules quickly. The change in molecular position will be reflected in the variation of the magnetic fields both spatially and temporarily. We can consider rotational tumbling (i.e. molecular rotations enhanced by collisions or tumbling of molecules against each other and hence τ_C is the rotational correlation time) as caused by random motion. Solving the diffusion problem for a randomly rotating molecule starting from Fick's law of diffusion in spherical coordinates and introducing spherical harmonics (e.g. $Y_0 = r^{-3}(1 - 3\cos^2\vartheta)$; $Y_1 = r^{-3}sin\vartheta cos\vartheta \exp{(i\varphi)}$; $Y_2 = r^{-3}\sin^2\vartheta \exp{(2i\varphi)}$) for dipolar coupling ($\gamma^2 r^{-3}(3\cos^2\vartheta - 1)$) yields the exponential autocorrelation function [6].

$$K(\tau) = K(0) \exp{(-|\tau|/\tau_C)} \tag{7}$$

Fourier theory tells that the power at frequency ω, i.e. the spectral density function, is given by the Lorentzian function as follows (using a constant C)

$$J(\omega) = \frac{C\,\tau_C}{1 + \omega^2\tau_C^2} \tag{8}$$

$J(\omega)$ indicates the fraction of molecules interacting or relaxing at frequency (ω) while the constant C reflects the strength of interaction between the molecule and the lattice at frequency (ω) and is related to the mean square value of the fluctuating magnetic fields and their characteristics. For example, although the dipolar fields are the most important in inducing relaxation, they are obviously not completely random which affect the assumption ($<B_x^2> = <B_y^2> = <B_z^2> = <B^2>$).

The spectral density function for different values of the correlation time τ_C is shown below in **Figure 1**. For T_1, the height of each curve indicates the strength of coupling between the spin and the lattice at that particular frequency, and hence the efficiency of relaxation.
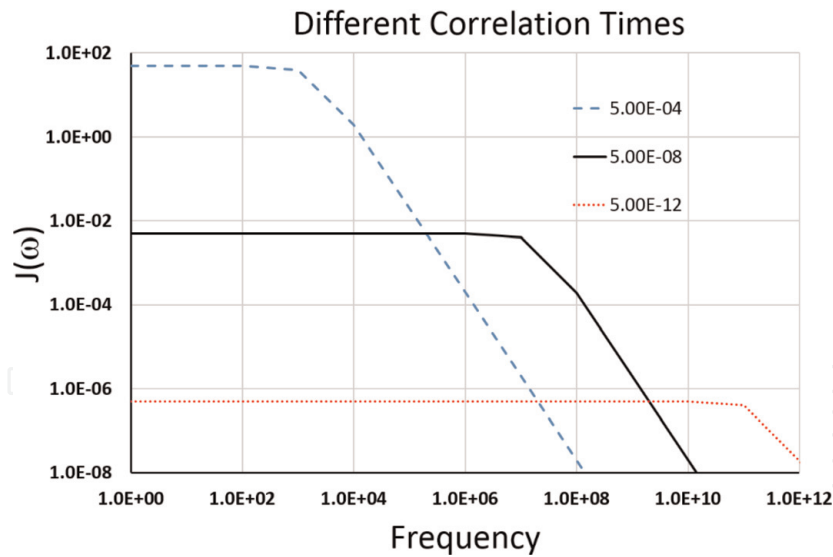
Figure 1.
The spectral density function for different values of the correlation time τ_C.

For identical spins the complete rotational relaxation rates ($1/T_1$ and $1/T_2$) induced by fluctuations at all three frequencies mentioned above (i.e. 0, ω_0, and also $2\omega_0$ where the two spins flip together) [7, 8] are given by

$$\frac{1}{T_1} = \frac{3}{10}\left(\frac{\mu_0}{4\pi}\right)^2 \frac{\gamma^4 h^2}{4\pi^2\, r^6}\, (J(\omega_0) + 4J(2\omega_0)) \tag{9}$$

$$= \frac{3}{10}\left(\frac{\mu_0}{4\pi}\right)^2 \frac{\gamma^4 h^2}{4\pi^2\, r^6}\left(\frac{\tau_C}{1+\omega_0^2\tau_C^2} + \frac{4\tau_C}{1+4\omega_0^2\tau_C^2}\right) \tag{10}$$

$$\frac{1}{T_2} = \frac{3}{40}\left(\frac{\mu_0}{4\pi}\right)^2 \frac{\gamma^4 h^2}{4\pi^2\, r^6}\, (3J(0) + 5J(\omega_0) + 2J(2\omega_0)) \tag{11}$$

$$= \frac{3}{20}\left(\frac{\mu_0}{4\pi}\right)^2 \frac{\gamma^4 h^2}{4\pi^2\, r^6}\left(3\tau_C + \frac{5\tau_C}{1+\omega_0^2\tau_C^2} + \frac{2\tau_C}{1+4\omega_0^2\tau_C^2}\right) \tag{12}$$

Different expressions are generated when considering translational motion involved in intermolecular motion with different values for the correlation times (τ_C) for both dipolar interactions and other mechanisms such as Quadrupole Relaxation, Scalar Relaxation, or Chemical Anisotropy. The equations provide asymptotic behavior for certain values of the important characteristic motional quantity ($\omega_0\tau_C$) which will be discussed later and the importance of the value $\left(\omega_0 \sim \frac{1}{\tau_C}\right)$ will be highlighted. The gyromagnetic ration (γ) points to the importance of using paramagnetic atoms (such as gadolinium and magnesium) in enhancing relaxation where the value of the electron's gyromagnetic ratio is larger than that for hydrogen by 658 times.

For example, for non-viscous liquids where the condition $\omega_0\, \tau_C \ll 1$ holds (i.e. τ_C is very small and the motion is very fast), both relaxation rates R_1 and R_2 ($R_I = 1/T_i$) are equal and are given by (for equal spin I)

$$R_1 = R_2 = \frac{2\gamma^4 h^2}{4\pi^2\, r^6}\, I(I+1)\tau_C \tag{13}$$

This regime is known as the motional averaging or extreme narrowing where relaxation is frequency independent. A brief introduction of relaxation enhancement due to the presence of paramagnetic atoms is given next in order to approach

the topic of magnetic nanoparticles. The term used to describe the efficacy of CA complexes in enhancing relaxation is "relaxivity" which is defined as the relaxation rate per unit concentration of CA.

4. Proton's relaxation due to paramagnetic complexes

The use of paramagnetic centers to reduce MRI relaxation times was first reported by Bloch in 1948 [9] and has been reviewed by many workers [10, 11]. We therefore only touch upon it briefly here in order to prepare the ground for the subject of magnetic nanoparticles as MRI contrast agents (CA). The most widely used paramagnetic atom is Gd (III) with its large magnetic moment (due to the seven umpired electrons), and relatively slow electronic relaxation rate, i.e. comparable to ω_0. Relaxation due to the fluctuating magnetic fields of these electronic spins through the dipole – dipole interaction can be classified into inner- and outer–sphere relaxation mechanisms. Solvent molecules (mostly water) can be bound to the paramagnetic compound in the first or second coordination sphere (directly or indirectly through other groups, respectively). These bound water protons can exchange with other water molecules and transfer the enhanced relaxation to protons from the bulk water. Factors that influence this intramolecular interaction mechanism (i.e. inner-sphere) are the rotational correlation time for the water molecule (τ_R) which is dependent on the rotational diffusion coefficient $\tau_R = 1/6D_R$), the electronic spin relaxation time T_{1e} and T_{2e}, and the water residence correlation time τ_m (the reciprocal of the exchange rate).

For intermolecular or outer-sphere interactions then translational diffusion in the vicinity of the paramagnetic ion plays a critical role. This mechanism will dominate T_2 relaxation when discussing magnetic nanoparticles later on over that of the inner sphere. We note that the dipole–dipole interaction strength decays very fast as $1/r^6$ Eq. (13). In view of the above and based on some assumptions the expressions for T_1 and T_2 in the above equations have been modified [12] to produce the Solomon-Bloembergen-Morgan (SBM) theory for relaxation. The expressions are complicated, however, and special cases can be considered where the picture is simplified. For example, if exchange rate is either very fast or very slow then averaging relaxation rates between the bound proton pool and the bulk water protons becomes efficient or not, respectively. The former then produces one overall relaxation rate while the latter is a sum of two rates [2]. The resonant-like increase in relaxation rate seen before when $\omega_0 \tau_C \sim 1$ is also present when the overall correlation rate $1/\tau_C$ approaches the Larmor frequency. This rate is now given by

$$\frac{1}{\tau_C} = \frac{1}{\tau_R} + \frac{1}{\tau_m} + \frac{1}{\tau_e} \tag{14}$$

τ_m is the residence correlation time, and τ_e is the electronic relaxation time, either T_{1e} or T_{2e}. The above discussion of paramagnetic relaxation enhancement clearly shows that there are many parameters that can be adjusted in order to adjust the inner-sphere relaxation process more than the outer-sphere one. Although, in general, both inner- and outer-processes contribute equally to overall proton relaxation, factors such as residence correlation time τ_m, hydration number, and the distance of closest approach (the smallest distance between water proton and the paramagnetic atom) can affect more the inner-sphere relaxation process. These parameters can be adjusted during the design and synthesis stages of the new contrast agent complexes in order to increase the efficiency of relaxation

enhancement. For example, linking multiple Gd complexes together increases the molecular weight, hence reducing mobility and increasing rotational correlation time. Furthermore, it will increase the dipole–dipole interaction by having more paramagnetic centers. The dependence of these parameters on the applied magnetic field is also important in determining the relaxivity of these complexes [13]. We will next describe relaxation enhancement due to MNP.

5. Magnetic nanoparticles (MNP)

Nanoparticles (NP) are materials that exhibit a size (largest dimension) in the range 1 to 100 nanometers (nm) and usually contain from several hundreds to 10^5 atoms. Recent advances in material synthesis science have enabled engineers and scientist to control the size, structure, and morphology of NP to high precision in the nano-scale where the classic laws of physics are different from that at the bulk scale. As the size of the particle decreases, the ratio of the surface area to the volume of the particle increases. For nanoparticles, this ratio becomes significantly large causing a large portion of the atoms to reside on the surface compared to those in the core of the particle. For example, for a particle of 1 µm in diameter, nearly 0.15% of its atoms are on the surface, while for a particle of 6 nm in diameter nearly 20% of its atoms are on the surface [14].

Magnetic materials are those materials that show a response to an applied magnetic field. The range of applications for this type of particles is very large and still increasing as synthesis methods improve further to control the size, size distribution, stoichiometry and the surface structure of NP. Applications include biomedical [15, 16], magnetic hyperthermia [17, 18], drug and peptide delivery systems and in the diagnosis and treatment of diseases [19, 20], magnetic fluids [20], water treatment [21], magnetic information and energy storage [22]. The application of magnetic nanoparticles also highly depends on the stability of the particles particularly for biomedical applications as efforts continue to protect the particles against oxidization and corrosion. Some of these challenges can be resolved by modifying the surface of the particle by coating with organic or inorganic materials such as starch, dextran or polyethylene glycol (PEG) [23, 24]. In addition to particles synthesized out of iron oxides, natural magnetized particles were also examined (red blood cell suspensions [25] and samples of liver or ferritin) to examine the different relaxation models mentioned below.

5.1 Physical and chemical properties of MNP

For MRI application as a Contrast Agent (CA) the interest is on superparamagnetic nanoparticles with a magnetic moment that is characterized by two important properties: firstly, a paramagnetic magnetism where the magnetic moment disappears when the magnetic field is removed; and secondly, a giant or super – ferromagnetic like – moment due to the alignment of spins along the applied magnetic field. If the particle is sufficiently reduced in size, then a state of single-domain is attained and it becomes superparamagnetic. In this state, the magnetic moment of the particle behaves as that of a single atom (like a paramagnet) but with much larger magnitude. Ferrimagnetic materials (such as magnetite Fe_3O_4 and maghemite γ-Fe_2O_3) are compounds of different atoms residing on different lattice sites with antiparallel magnetic moments. In these materials, the magnetic moments do not cancel out since they have different magnitudes which results in a net spontaneous magnetic moment. When placed in a magnetic field,

antiferromagnetic and ferrimagnetic materials show a behavior similar to that of ferromagnetic ones [14].

Iron has been used by many researchers to synthesize MRI CA either as iron metals [26], iron oxides [27] and ferrites substituted by other elements such as Zn, Mn, and Gd [28, 29], or indeed CA that are based on Gd or gold [30]. The addition of other elements was either to modify the magnetic moment or indeed to add another function to the CA such as heating in hyperthermia. There are many chemical and physical synthesis methods for the preparation of iron oxide nanoparticles with various degrees of control over the properties of the final product. Perhaps the most widely used method, due to its simplicity, speed, and relatively low cost, is the coprecipitation of Fe^{2+} and Fe^{3+} aqueous alkaline solutions by adding a base. The iron compounds formed by this method may have various degrees of compositions and crystal structure. The particles produced are quasi-spherical in shape, however, polydisperse in size especially if stabilizing agents such as dextran, PEG, or polysaccharides are not used. Stabilization of the ferrofluid using these agents is important in order to prevent particles from clustering. Particles tend to agglomerate in order to reduce the interfacial tension which is large due to the large surface to volume ration of nanoparticles. One of the most important characteristics of MNP (if not the most important) for medical applications is particle monodispersity. Failing to preserve monodispersity will defeat the objectives of designing and implementing any synthesis method and indeed the route of application because almost every step involved rely on the assumption of a single valued parameter rather than a range of values i.e. a distribution, at least until recently. For example, when quantifying an application of MNP a single value for each of radius, magnetization, susceptibility is given. Further difficulties ensue when clustering or agglomeration of nanoparticles exists emphasizing the importance of determining the particle radius as demonstrated by many studies such as those mentioned in ([31–33]). For MRI a more detailed study [34] of the different degrees of agglomeration induced by many types of coating concluded that clustering was the more dominant factor in changing relaxivity over other factors such as diffusion and the distance of water protons from the magnetic core.

For MRI at typical clinical magnetic fields the magnetic moment and the size of the MNP will ultimately decide the CA relaxivity and indeed its biodistribution. Therefore, it is imperative to control the aggregation of the crystals in order to define the sample size distribution. This is usually done by modifying the surface layer of the MNP, e.g. by adding some coating materials or surfactants or by changing the surface charge. Care must be exercised when doing so because the effective size or the hydrodynamic radius will also be affected. Another consequence to this will be the modification of the distance of closest approach between water protons and the MNP which reduces relaxivity. Furthermore, these mostly polymer materials will have an effective diffusion coefficient which is smaller than that of the bulk water and indeed may not have a single value across the full thickness of the coating layer. For example, we may expect the proton ability to diffuse through layers close to the metal core of the coated or aggregated MNP to be smaller than its ability in regions at the exterior regions of the coating layer close to the bulk water. Coating also leads to ambiguity in determining the magnetization, since magnetization is the magnetic moment per unit volume. The latter may not be accurately defined or indeed measurement-method dependent. Of course, further ambiguities may arise when vectorizing the coated MNP for biomedical applications such as cellular tracking and targeting in molecular imaging. The schematic given in **Figure 2** shows different possible particle geometries according to clustering and distance between different clusters within one large agglomerated coated particle.
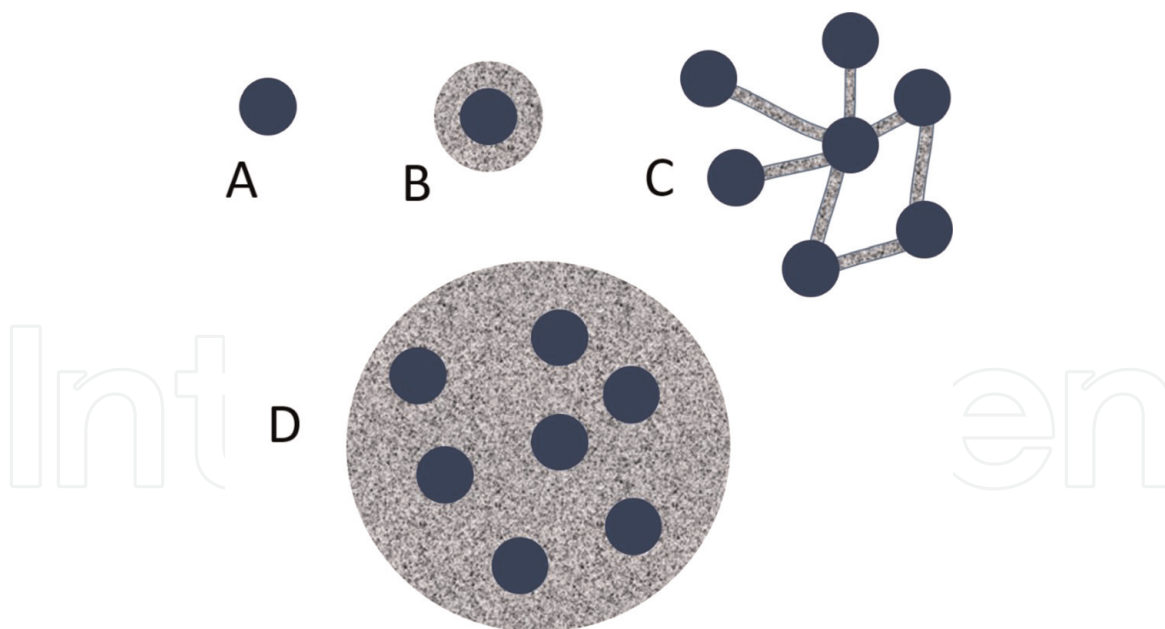
Figure 2.
Different geometries for MNP that are not agglomerated (A) uncoated; and (B) coated; while (C) connected particles (uncoated) by polymers while in D) can be considered one large agglomerated particle with a much larger hydrodynamic size due to the coating.

5.2 Proton's relaxation by MNP

Due to the ability to assemble many (e.g. 1000s) of iron atoms into the MNP the magnetic moment associated with ferro- or super-paramagnetic nanoparticles is much bigger than that associated with a single paramagnetic atom or even few linked Gd complexes. If comparable relaxation enhancement can be produced by a smaller mass of CA material, then efficiency and safety can be improved, and the amount of chemical dose administered into humans is reduced. For superparamagnetic NP the outer-sphere relaxation contribution dominates over the inner-sphere one (recall that in the paramagnetic case discussed before both mechanisms contribute comparably). Another distinction from the paramagnetic centers, is that the modulation of the dipolar interactions is provided by Néel's relaxation of the MNP (instead of the electronic relaxation) characterized by the correlation time τ_N; and possibly to a smaller extent by the Brownian relaxation characterized by the correlation time τ_D. Protons diffuse through non-fluctuating magnetic field gradients created by the mean crystal moment [35–36] which is locked along the external magnetic field. The diffusion process depends on the particle size, the solvent viscosity and temperature while the two MNP relaxation processes, depends on the size and anisotropy energy of the particle which increases exponentially with the particle volume.

Early studies of NMR relaxation as a function of field strength or frequency, known as NMR Dispersion (NMRD) curves discussed the importance of the anisotropy energy at very low fields [37]. The model successfully explained the experimental results for large superparamagnetic iron oxide (SPIO) crystals (radius ~15 nm) at high fields but failed to agree with relaxation results for smaller particles (ultra-SPIO or USPIO ~5 nm) especially in the low field range where dispersion (i.e. inflection point in the dispersion curve) in the longitudinal NMRD curves occurs [38]. For MRI at current fields [14], however, and especially at MNP typical size used in biomedical applications, Curie relaxation dominates where the NP magnet is locked along B_0 direction and the relaxation rates are then given by (under certain conditions—see next section) the following equations (similar to

Eq. (22–24) in [39]; Eq. (20) and (21) ignoring Freed's contribution in [40]; Eq. (2) and (3) in [41]):

$$\frac{1}{T_1} = \frac{32\pi}{135000} \frac{N_A[M]}{RD} \left(\frac{\gamma\mu_0}{4\pi}\right)^2 \left\{\frac{3}{2} J_A\left(\sqrt{2\omega_I\tau_D}\right)\right\} <\mu_Z>^2 \qquad (15)$$

$$\frac{1}{T_2} = \frac{32\pi}{135000} \frac{N_A[M]}{RD} \left(\frac{\gamma\mu_0}{4\pi}\right)^2 \left\{\frac{3}{2} J_A\left(\sqrt{2\omega_I\tau_D}\right) + J_A(0)\right\} <\mu_Z>^2 \qquad (16)$$

ω_I is the proton's Larmor frequency, μ_Z is the magnetic moment component along the applied field, N_A is Avogadro's number, and J_A is Ayant's density spectral function given by

$$J_A(z) = \frac{1 + 5z/8 + 5z^2/8}{1 + z + z^2 + \frac{z^3}{6} + 4z^4/81 + z^5/81 + z^6/648} \qquad (17)$$

For high fields when ω_I becomes very large ($J_A(z) \to$ zero) and using the volumetric particle fraction f instead of the molar concentration $[M]$ (moles/liter) the relaxation rates can be written as

$$1/_{T_1} \to zero \qquad (18)$$

$$1/_{T_2} = \frac{16}{45} f(\Delta\omega)^2 \tau_D \qquad (19)$$

$\Delta\omega$ is the r.m.s. Larmor frequency experienced by the proton at the surface of the particle of radius R and is given by [42, 43]

$$\Delta\omega = \sqrt{4/5}\mu_0 M \frac{\gamma}{3} \qquad (20)$$

$\Delta\omega$ depends only on the material magnetization [43] and not the size of the particle, for example, magnetite has $\Delta\omega$ = 3.48 × 10^7 rads/s. The magnetic frequency can of course be represented in terms of the magnitude of the component of the equatorial magnetic field (B_{eq}) parallel to the external field B_0 using the Larmor relationship. Magnetite's frequency will then correspond to an equatorial magnetic field B_{eq} = 1.3 kG.

5.3 Motional regimes for T$_2$

We consider in detail the effect of the diffusing motion of the water protons as they move around the MNP and sample the variations in their magnetic fields. The tortuous nature of the Brownian motion means that the water proton encounters the MNP many times in order to lose phase coherence, i.e. relax significantly or equivalently, the motion of the proton has to be very fast in order to experience and average the magnetic fields of many nanoparticles [42]. The water proton is neither confined to the magnetic field of one MNP nor is completely relaxed by diffusing around it [37]. This process defines the dynamic frequency scale or diffusional rate $1/\tau_D = D/d^2$ (notice the use of "d", the distance of closest approach, or "R", the radius of the nanoparticle by many researchers). Obviously, the strength of the magnetic dephasing center has to be taken into account and this is characterized by the magnetic frequency scale which represents the efficiency by which the MNP relaxes a nearby proton as defined above in Eq. (14) [44].

The choice of the theoretical model of T_2 relaxation depends on both the size of the particles (*i.e.*, mobility) and the magnitude of the magnetic moment (*i.e.*, the

dephasing effect due to field inhomogeneity) through the product parameter $\Delta\omega \, \tau_D$. When the diffusional motion is very fast such that one MNP is unable to completely relax the protons the condition for the motional averaged regime (MAR) is fulfilled $1/\tau_D \gg \Delta\omega$ and Eq. (19) represents the transverse relaxation rate [14].

The $1/T_2$ relaxation rate continues to increase with increasing particle size (or linearly with R^2) until reaching an asymptotic limit in $1/T_2$ (both $1/T_2$ and $1/T_2{}^*$ are equal and independent of echo time τ_{CP} where τ_{CP} is half the echo time for a single (Hahn) spin-echo or half the interval between successive 180° RF pulses in a CPMG sequence) when further particle size increase causes the breakdown of the MAR condition. The limited spins mobility leads to the saturation of $1/T_2{}^*$ value with further particle size increases as given by the static dephasing regime (SDR) where the protons appear less mobile, or static [43, 45, 46]. Therefore, when $\Delta\omega \, \tau_D \gg 1$, spins relax in the magnetic field gradients created by nearby weakly or strongly magnetized particles and the diffusion coefficient becomes irrelevant. The expression for $1/T_2$ in the SDR regime is given by

$$1/_{T_2} = \frac{2\pi}{\sqrt{27}} \, f \, \Delta\omega \qquad (21)$$

For large particles, or agglomeration of particles [47], where the refocusing RF pulses are not effective and the diffusion time τ_D is larger than a characteristic time τ_L given by

$$\tau_L = \left(\frac{1.49}{\Delta\omega}\right) x^{1/3} \, (1.52 + f \, x)^{5/3} \qquad (22)$$

$x = \Delta\omega \, \tau_{CP}$, the theoretical model for $T2$, known as the echo limited regime (ELR), applies and is given by

$$1/T2^{ELR} = 1.8 f \, x^{1/3} \, (1.52 + f \, x)^{5/3} / \tau_D \qquad (23)$$

It should be noted that the accuracy of the above model for vary large particles is not very high and relaxation cannot just be described by a single exponential curve. This is so because dephasing is often described by a very fast component close to the surface of the particle and another slower component at farther distances.

Monte Carlo (MC) numerical simulation was used by many researchers to study T_2 relaxation [44, 48, 49] for both spherical and cylindrical particle geometry. To demonstrate the applicability of the above models we simulated transverse relaxation due to the presence of spherical MNP for both T_2 and T_2. We investigated relaxation under the different motional regimes and particle concentration. **Figure 3** shows $1/T_2$ simulations for four values of the echo time τ_{CP} ranging from 3.13×10^{-05} to 2.50×10^{-04} seconds and a volume fraction $f = 1 \times 10^{-05}$. The theoretical values for MAR and SDR are shown as well as the four curves for large particle size in the ELR regime. Available models for the latter range give an overestimate for the simulation.

Values of $1/T_2$ simulations are shown in **Figure 4** below (for the same parameters used in **Figure 3** above). The agreement between spin-echo and gradient-echo data is evident for small particles within the MAR regime while the upper limit reached by all larger particles for all echo times is clearly demonstrated within the SDR regime consistent with Eq. (21) above.

Simulation can aid in understanding the relaxation mechanisms and developing new models by investigating the effect of different environments, particle sizes, coating types, *etc.* under both spin- and gradient-echo experimental conditions. The
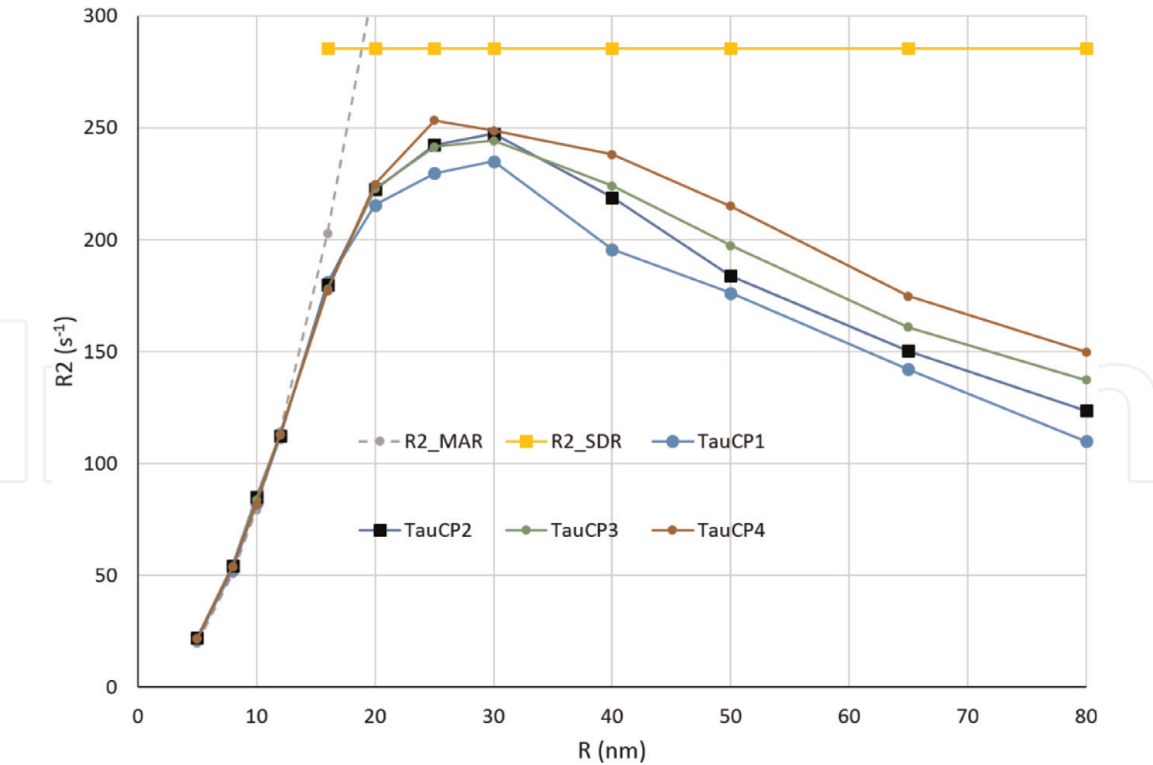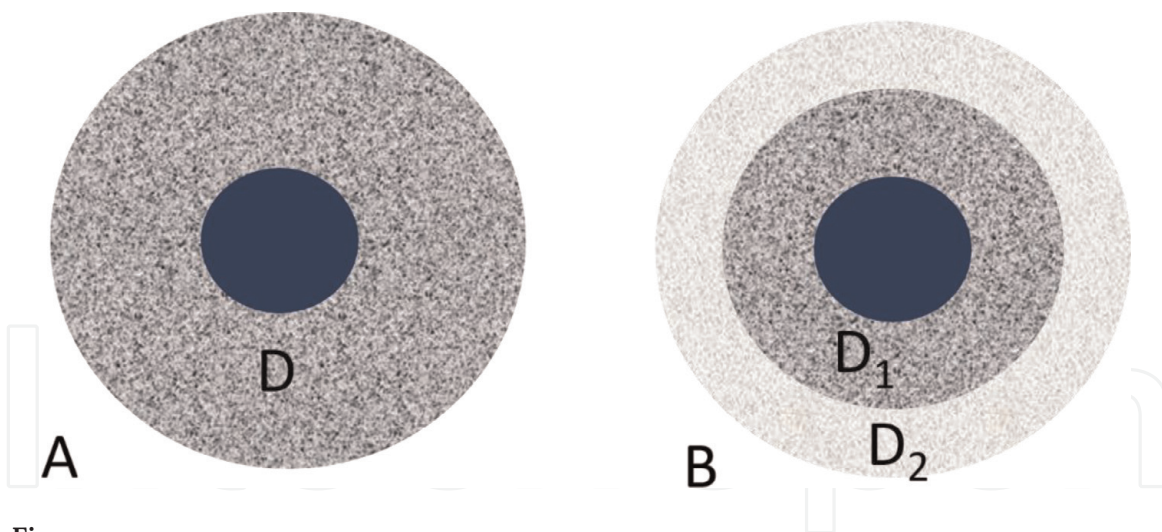
Figure 3.
1/T$_2$ simulations for four small values of the echo time τ_{CP}: 3.13×10^{-05}, 6.25×10^{-05} 1.25×10^{-04}, to 2.50×10^{-04} s. All particles used were spherical of the same size and the volume fraction $f = 1 \times 10^{-05}$.
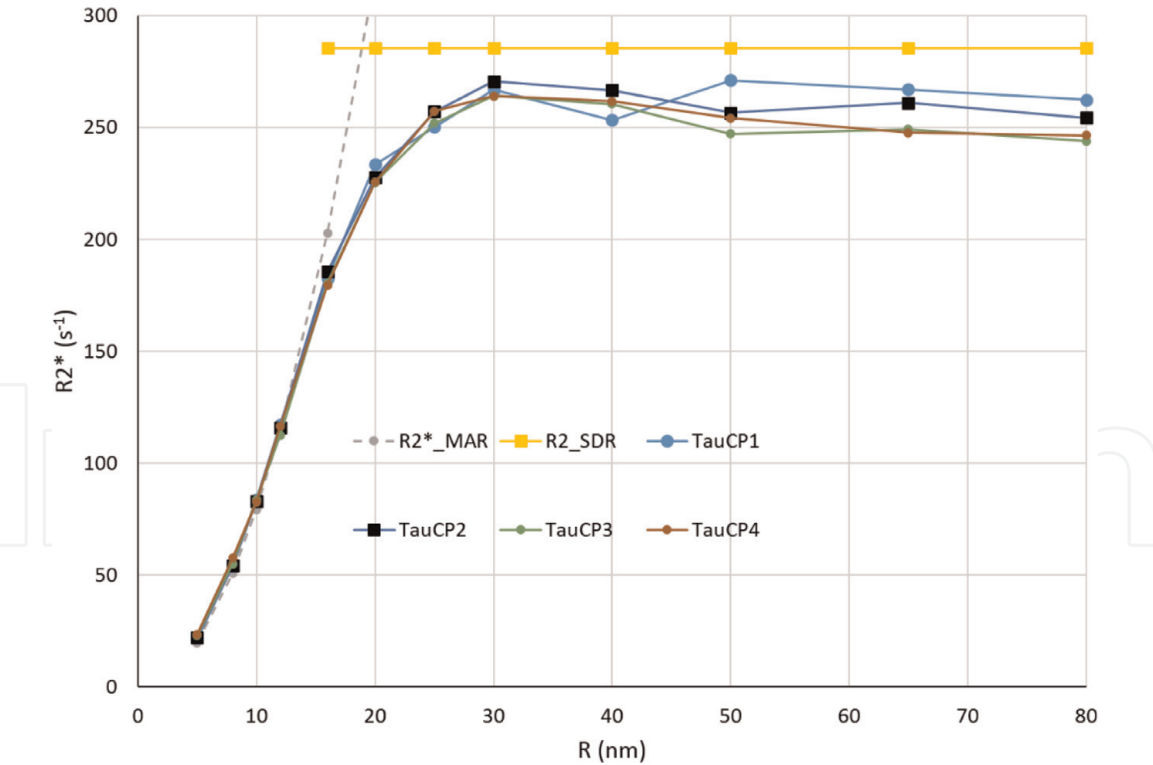
Figure 4.
1/T$_2^*$ simulations for four small values of echo time τ_{CP}: 3.13×10^{-05}, 6.25×10^{-05} 1.25×10^{-04}, to 2.50×10^{-04} s. All particles used were spherical of the same size and the volume fraction $f = 1 \times 10^{-05}$.

role of PEG coating can also be examined by specifying a regional zone around the magnetic core with a different coefficient of diffusion to that of the bulk water. Indeed, layers of coating material of different mobility can also be studied in order to simulate the environment more realistically as shown in **Figure 5**. Relaxivity was shown to decrease in [50, 51] due to increasing the water protons' distance of closest

Figure 5.
Different models for the effect of the coating layer depending on the values of the diffusion coefficient according to position between the core and the bulk water. Simulations can be used to investigate the ensuing effect on relaxation.

approach by the coating layer and reduced diffusion coefficient. However, increased T_1 relaxivity was demonstrated in [51] explained by longer proton's residence time associated with the reduced diffusion coefficient.

5.4 Core-shell structures

We have seen that the magnetic moment and the size of the MNP play the most important role in determining MRI relaxivity. Therefore, it is important that the experimental determination of these quantities is accurate and independent of each other, if possible. If the sample is polydisperse, and depending on the width of the size distribution, then it may not be possible to fit the magnetization data to a single Langevin curve [52, 53]. Particle size distribution, in addition to the existence of multi-magnetization phases (e.g. more than one superparamagnetic magnetic moment component), play an important role in accurately determining the particle's magnetic moment [54]. The isolation of phases during synthesis or the existence of a dead shell layer (e.g., paramagnetic) are necessary to explain the widely reported lack of saturation of the magnetization curve even at very large applied fields [54]. A closely related topic is core-shell structures. In comparison to a single core of iron-oxide nanoparticles, core-shell structured iron/iron-oxide nanoparticles offer a much stronger T_2 shortening effect than that of iron-oxide with the same core size [55, 56]. Multifunctional NP benefit from the ability to combine iron or other metals to the conventional iron oxide material. Combined hyperthermia and MRI rely on doping iron oxide particles with metals such as Mn and Gd in order to control their thermodynamic properties [32]. Multimodality imaging offers other imaging modality in addition to MRI to help in improving the diagnostic information [56]. Recent advances in synthesis method opened the way for a better control over the particle morphology. Cubic and flower-shaped particles offer higher magnetization values through anisotropy and larger surface to volume ratios [57]. Cubic nanoparticles can have a higher degree of crystallinity and relaxivity (four times higher) than their spherical counterparts [58].

6. Conclusions

Superparamagnetic particles mostly synthesized from iron oxide exhibit large magnetic moment compared to the Gd-chelates conventionally used as MRI

contrast agents. The ability to control the structure, morphology, size, and size distribution is critical to the optimum application of these magnetic nanoparticles as MRI relaxation enhancing centers. Further coating and functionalization of the surface of these particles enable their use as multifunctional particles in cancer treatment or multimodality imaging. Recent synthesis methods have produced cubic and assembled particles with improved performance in terms of larger magnetic moment which offers not only higher MRI relaxivity but also reduced dose of injected material.

Author details

Bashar Issa[1]* and Ihab M. Obaidat[2]

1 Department of Medical Diagnostic Imaging, College of Health Sciences, University of Sharjah, Sharjah, UAE

2 Department of Physics, College of Science, United Arab Emirates University, Al Ain, UAE

*Address all correspondence to: bissa@sharjah.ac.ae

IntechOpen

References

[1] Damadian R. Tumor detection by nuclear magnetic resonance. Science. 1971;**171**(3976):1151-1153. Available from: http://www.ncbi.nlm.nih.gov/pubmed/5544870

[2] Callaghan PT. Principles of Nuclear Magnetic Resonance Microscopy. England: Oxford University Press; 1991

[3] Andrew ER. Nuclear Magnetic Resonance. Cambridge: University Press; 1955. 114 p

[4] Farrar TC, Becker ED. Pulse and Fourier Transform NMR. New york and London: Academic Press; 1971. pp. 34-45. Available from: http://www.sciencedirect.com/science/article/pii/B9780080918129500089

[5] Doob JL. The elementary Gaussian processes. Annals of Mathematical Statistics. 1944;**15**(3):229-282

[6] Levitt MH. Spin Dynamics Basics of Nuclear Magnetic Resonance. 2 ed. Chichester, England: John Wiley & Sons Ltd; 2008

[7] Solomon I. Relaxation processes in a system of two spins. Physics Review. 1955;**99**:559

[8] Lauffer RB. Paramagnetic metal complexes as water proton relaxation agents for NMR imaging: Theory and design. Chemical Reviews. 1987;**87**(5):901-927. DOI: 10.1021/cr00081a003

[9] Bloch F, Hansen WW, Packard M. The nuclear induction experiment. Physics Review. 1946;**70**:474

[10] Caravan P, Ellison JJ, McMurry TJ, Lauffer RB. Gadolinium(III) chelates as MRI contrast agents: Structure, dynamics, and applications. Chemical Reviews. 1999;**99**(9):2293-2352. DOI: 10.1021/cr980440x

[11] Sherry AD, Caravan P, Lenkinski RE. Primer on gadolinium chemistry. Journal of Magnetic Resonance Imaging. 2009;**30**(6):1240-1248

[12] Kowalewski J. In: Grant DM, Harris RK, editors. Encyclopedia of Nuclear Magnetic Resonance. Chichester: John Wiley & Sons, Ltd.; 1996. pp. 3456-3462

[13] Trattnig S, Pinker K, Ba-Ssalamah AN-HI. The optimal use of contrast agents at high field MRI. European Radiology. 2006;**16**:1280-1287

[14] Issa B, Obaidat IM, Albiss BA, Haik Y. Magnetic nanoparticles: Surface effects and properties related to biomedicine applications. International Journal of Molecular Sciences. 2013;**14**(11):21266-21305

[15] Kolhatkar AG, Jamison AC, Litvinov D, Willson RCLT. Tuning the magnetic properties of nanoparticles. International Journal of Molecular Sciences. 2013;**14**:15977-16009

[16] Lübbe AS, Bergemann C, Riess H, Lãbbe AS, Schriever F, Reichardt P, et al. Clinical experiences with magnetic drug targeting : A phase I study with 4′-epidoxorubicin in 14 patients with advanced solid tumors in 14 patients with advanced solid tumors. Cancer Research. 1996:4686-4693

[17] Ito A, Honda H, Kobayashi T. Cancer immunotherapy based on intracellular hyperthermia using magnetite nanoparticles: A novel concept of "heat-controlled necrosis" with heat shock protein expression. Cancer Immunology, Immunotherapy. 2006;**55**:320-328

[18] Nobuto H, Sugita T, Kubo T, Shimose S, Yasunaga Y, Murakami T, et al. Evaluation of systemic chemotherapy with magnetic liposomal doxorubicin and a dipole external

electromagnet. International Journal of Cancer. 2004;**109**(4):627-635. Available from: http://www.ncbi.nlm.nih.gov/pub med/14991586

[19] Ruysschaert T, Paquereau L, Winterhalter M, Fournier D. Stabilization of liposomes through enzymatic polymerization of DNA. Nano Letters. 2006;**6**:2755-2757

[20] Taylor R, Coulombe S, Otanicar T, Phelan P, Gunawan A, Lv W, et al. Small particles, big impacts: A review of the diverse applications of nanofluids. Journal of Applied Physics. 2013;**113**: 011301

[21] Yavuz C, Mayo J, Yu W, Prakash A, Falkner J, Yean S, et al. Low-field magnetic separation of monodisperse Fe3O4 nanocrystals. Science (80-). 2006;**314**:964-967

[22] Singamaneni S, Bliznyuk V, Binekc C, Tsymbalc E. Magnetic nanoparticles: Recent advances in synthesis, self-assembly and applications. Journal of Materials Chemistry. 2011;**21**: 16819-16845

[23] Di Marco M, Guilbert I, Port M, Robic C, Couvreur P, Dubernet C. Colloidal stability of ultrasmall superparamagnetic iron oxide (USPIO) particles with different coatings. International Journal of Pharmaceutics. 2007;**331**:197-203

[24] Gupta AK, Gupta M. Synthesis and surface engineering of iron oxide nanoparticles for biomedical applications. Biomaterials. 2005;**26**(18): 3995-4021. Available from: http://www. ncbi.nlm.nih.gov/pubmed/15626447

[25] Lisitza N, Warren W, Song Y-Q. Study of diffusion in erythrocyte suspension using internal magnetic field inhomogeneity. Journal of Magnetic Resonance. 2007;**187**:146-154

[26] Bautista MC, Bomati-Miguel O, Zhao X, Morales MP, González-Carreño T, De Alejo RP, et al. Comparative study of ferrofluids based on dextran-coated iron oxide and metal nanoparticles for contrast agents in magnetic resonance imaging. Nanotechnology. 2004;**15**(4): S154-S159. Available from: http://stacks. iop.org/0957-4484/15/i=4/a=008?key=c rossref.adfd4debc6b423edb6d2c 867057ef978

[27] Elias A, Tsourkas A. Imaging circulating cells and lymphoid tissues with iron oxide nanoparticles. Hematology. 2009;**2009**:720-726

[28] Issa B, Obaidat IM, Hejasee RH, Qadri S, Haik Y. NMR relaxation in systems with magnetic nanoparticles: A temperature study. Journal of Magnetic Resonance Imaging. 2014;**39**(3):648-655

[29] Hejase H, Hayek SS, Qadri S, Haik Y. MnZnFe nanoparticles for self-controlled magnetic hyperthermia. Journal of Magnetism and Magnetic Materials. 2012;**324**(22):3620-3628. Available from: http://www.scienced irect.com/science/article/pii/ S0304885312002983

[30] Heitsch A, Smith D, Patel R, Ress D, Korgel B. Multifunctional particles: Magnetic nanocrystals and gold nanorods coated with fluorescent dye-doped silica shells. Journal of Solid State Chemistry. 2008;**181**:1590-1599